Atomic layer deposition of ultrathin platinum films on tungsten atomic layer deposition adhesion layers: Application to high surface area substrates

Joel W. Clancey and Andrew S. Cavanagh
Department of Chemistry and Biochemistry, University of Colorado, Boulder, Colorado 80309

Ratandeep S. Kukreja and Anusorn Kongkanand
General Motors, Global Product Development, Pontiac, Michigan 48340

Steven M. George[a)]
Department of Chemistry and Biochemistry, University of Colorado, Boulder, Colorado 80309 and Department of Mechanical Engineering, University of Colorado, Boulder, Colorado 80309

(Received 3 September 2014; accepted 31 October 2014; published 1 December 2014)

Platinum (Pt) atomic layer deposition (ALD) usually yields Pt nanoparticles during initial film growth. In contrast, deposition of continuous and ultrathin Pt films is needed for many important applications, such as the oxygen reduction reaction in polymer electrolyte membrane (PEM) fuel cells. A continuous and high radius of curvature Pt film is more stable and has a higher area-specific activity than the Pt nanoparticles commonly used in PEM fuel cells. However, the Pt film must be ultrathin and have a large surface area to be cost effective. In this paper, a review of earlier Pt ALD studies on flat substrates is presented that demonstrates that tungsten, with a higher surface energy than platinum, can serve as an adhesion layer to achieve Pt ALD films that are continuous at ultrathin thicknesses of ~1.5 nm. This work utilized $MeCpPtMe_3$ and H_2 plasma as the Pt ALD reactants. The deposition of continuous and ultrathin Pt ALD films using $MeCpPtMe_3$ and H_2 plasma as the reactants is then studied on two high surface area substrate materials: TiO_2 nanoparticles and 3M nanostructured thin film (NSTF). Transmission electron microscopy (TEM) showed uniform and continuous Pt films with thicknesses of ~4 nm on the TiO_2 nanoparticles. TEM with electron energy loss spectroscopy analysis revealed W ALD and Pt ALD films with thicknesses of ~3 nm that were continuous and conformal on the high aspect ratio NSTF substrates. These results demonstrate that cost effective use of Pt ALD on high surface area substrates is possible for PEM fuel cells. © *2014 American Vacuum Society*. [http://dx.doi.org/10.1116/1.4901459]

I. INTRODUCTION

The efficient use of precious catalytic metals, such as platinum (Pt), is critical for many applications. One such application is the use of Pt to catalyze the oxygen reduction reaction (ORR) in polymer electrolyte membrane (PEM) fuel cells.[1–3] The PEM fuel cell has become a strong candidate to replace the internal combustion engine because of its high efficiency and nonpolluting emissions. Platinum metal is the key catalyst in both the anode and cathode electrodes of the PEM fuel cell.[1–5] However, platinum is expensive and must be used in PEM fuel cells as efficiently and effectively as possible.

The current strategy to fabricate efficient Pt electrocatalysts is to disperse 2–5 nm diameter Pt nanoparticles on high surface area carbon black.[1–5] Although the Pt nanoparticles yield a large catalytic surface area, they are unstable due to dissolution and Ostwald ripening processes that lead to performance loss and decreased fuel cell lifetime.[6–9] Pt nanoparticles also have a low area-specific activity toward the ORR. In contrast, Pt surfaces with a large radius of curvature of ≥500 nm have a 5–10 fold higher area-specific activity toward the ORR compared with the surfaces of 2–5 nm diameter Pt nanoparticles.[3] Unfortunately, Pt particles with this large radius of curvature are expensive and also have a low mass activity because only the surface Pt atoms participate in catalysis. One solution is to deposit an ultrathin and continuous Pt film on an inexpensive and high surface area core material to obtain a more stable, cost effective, and active catalyst.[10]

Atomic layer deposition (ALD) is a self-limiting, gas-phase growth technique capable of depositing ultrathin and conformal metal and metal oxide films on high aspect ratio substrates.[11,12] The growth of ALD films occurs through sequential surface reactions that typically lead to a layer-by-layer (Frank van der Merwe) growth mechanism when enough chemically active species exist on the initial substrate surface. The surface reactions can be thermally driven using elevated reaction temperatures or assisted by a plasma that generates reactive species to drive the surface reactions.[12,13]

Pt ALD on metal oxides does not typically result in the layer-by-layer growth mechanism. Rather, Pt ALD leads to the growth of Pt nanoparticles as described by islandlike (Volmer-Weber) growth. The ALD of Pt nanoparticles has been demonstrated using a variety of Pt precursors and different reactive gases on metal oxide supports.[14–27] Examples are Pt ALD using either trimethyl(methylcyclopentadienyl) platinum ($MeCpPtMe_3$) and O_2 as the reactants or hexafluoroacetylacetonate ($Pt(hfac)_2$) and formalin as the reactants.[26,27] Figure 1 shows a transmission electron microscopy (TEM)

a)Electronic mail: Steven.George@Colorado.Edu

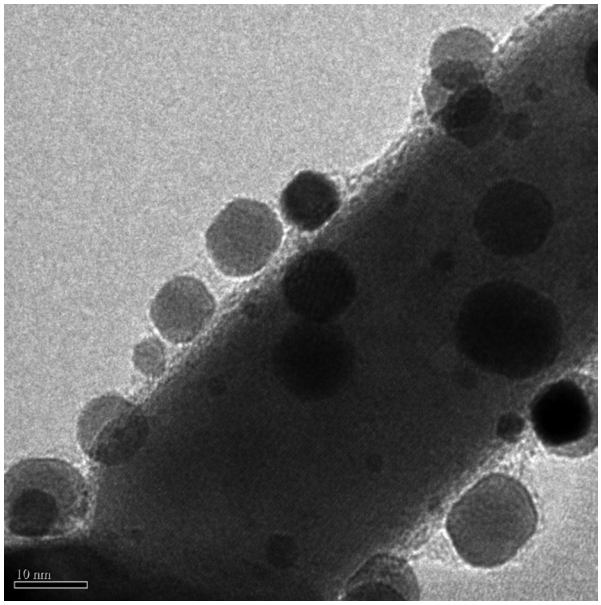

FIG. 1. TEM image of Pt nanoparticles on a WO_x nanorod. The Pt nanoparticles were deposited with 170 Pt ALD cycles using $Pt(hfac)_2$ and formalin as the reactants at 200 °C. Reprinted with permission from Anderson *et al.*, J. Phys. Chem. C **118**, 8960 (2014). Copyright 2014, American Chemical Society.

image of nearly spherical Pt nanoparticles grown on a tungsten oxide (WO_x) nanorod using platinum hexafluoroacetylacetonate [$Pt(hfac)_2$] and formalin as the reactants at 200 °C.[27]

The islandlike growth of Pt ALD on metal oxide surfaces is largely due to the poor wettability of Pt caused by the difference in surface energy between the Pt and metal oxide substrate.[28] Platinum has a high surface energy of ~2.5 J/m^2 while most metal oxides have surface energies in the range of 0.6–2 J/m^2.[29,30] When Pt ALD nucleates on an oxide surface, Pt nanoclusters initially form to minimize their surface area to lower their surface energy. A continuous Pt ALD film is achieved following many ALD cycles after the coalescence of the Pt nanoparticles.

One way to enhance Pt wetting is to deposit the Pt ALD on a surface that has a higher surface energy than Pt itself.[10] Tungsten metal has a surface energy of ~3.3 J/m^2.[30] This surface energy is higher than the surface energy of any other metal with the possible exception of rhenium.[30] We have found that W ALD can be grown as continuous, ultrathin films on Al_2O_3 ALD surfaces as a result of some unusual surface chemistry.[31–35] Platinum can then wet the W ALD surface because the Pt film will lower the system surface energy.

In this paper, we review the work on the nucleation and growth of ultrathin Pt ALD on W ALD adhesion layers using $MeCpPtMe_3$ and H_2 plasma. We then build upon these results by depositing ultrathin and continuous Pt ALD films on high surface area substrates. The two high surface area substrates are TiO_2 nanoparticles and organic whiskers known as 3M nanostructured thin film (NSTF).[1,36–38] Both of these substrates are possible supports for PEM fuel cell electrocatalysts because they are inexpensive and more resistant to electrochemical corrosion than carbon black.[36–41]

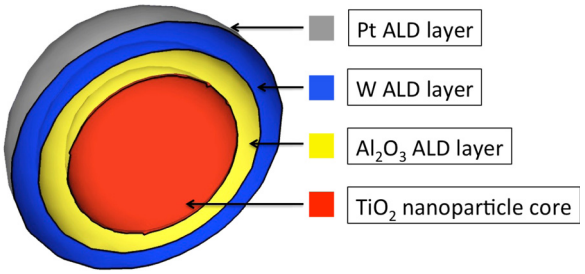

FIG. 2. (Color online) Schematic depicting a TiO_2 nanoparticle with Al_2O_3 ALD, W ALD, and Pt ALD layers forming a multilayer shell around the TiO_2 nanoparticle.

A sequence of ALD processes is required to deposit ultrathin and continuous Pt films. Figure 2 shows a cartoon depicting the sequence of ALD materials leading to an ultrathin Pt ALD film on a TiO_2 nanoparticle. The Al_2O_3 ALD layer facilitates the growth of ultrathin and continuous W ALD layers.[31] The W ALD layer then allows for the growth of ultrathin and continuous Pt ALD layers.[10] This scheme yields Pt ALD films with a large radius of curvature for efficient ORR catalytic activity without requiring the Pt layer to support itself.

II. EXPERIMENT

A. ALD reactors

Depositions were performed in three separate ALD reactors depending on the substrate material. For ALD on the TiO_2 nanoparticles, an open-ended rotary reactor was used that is attached to a plasma source. This reactor was used for the Al_2O_3, W, and Pt ALD reactions at 180, 120, and 150 °C, respectively. For ALD on the 3M NSTF substrate material, a viscous flow ALD reactor was employed to deposit the Al_2O_3 and W ALD adhesion layers at 120 °C.[31] A plasma-assisted ALD reactor was then used to deposit the Pt ALD at 120 °C.[42]

A plasma-assisted open-ended rotary ALD reactor was used for the TiO_2 nanoparticle substrates. This reactor combines concepts from a previous rotary reactor design and a remote plasma-assisted ALD system.[43–45] The open-ended rotary ALD reactor was mounted on an adjustable frame that allowed the angle of the reactor to be varied to keep the particles confined in the rotary reactor. The TiO_2 nanopowder was contained in a stainless steel cylinder that had one end completely open to the precursor manifold and remote inductively coupled plasma (ICP) source. The open end of the cylinder improved gas conductance during ALD and maximized the H radical exposure during H_2 plasma-assisted ALD.

The open-ended cylinder was attached to a feedthrough shaft that was connected to the rear of the reactor and rotated using a magnetically coupled motor and DC power supply (BK Precision 1670 A). The cylinder could be rotated at speeds as high as ~250 revolutions per minute (RPM) to agitate the powders. The plasma source was a remote ICP consisting of a quartz tube (6.0 cm inner diameter × 21.6 cm long) surrounded by a copper helical coil. The ICP was

generated using the same radio frequency (RF) generator and impedance matching network as described previously.[10,42] The ICP source was separated from the reactor chamber by a gate valve to prevent metal deposition inside the quartz tube during plasma-assisted ALD. This open-ended rotary ALD reactor will be described more completely in a future publication.

The viscous flow reactor used to deposit Al_2O_3 and W ALD on the 3M NSTF substrate was described in detail elsewhere.[31] Briefly, this hot wall ALD reactor consists of a stainless steel tube (3.5 cm inner diameter × 45 cm long) with seven precursor gas lines feeding in through a custom built 2.75 in. Conflat to 1/4 in. VCR adapter. Nitrogen carrier gas (Airgas, UHP) was flowed to maintain a pressure of ~1 Torr in the reactor flow tube when pumped on using an Alcatel 2010 rotary vane pump. Fill tanks for both the Si_2H_6 and WF_6 precursors were used to control the W ALD film growth at 120 °C. Each precursor was allowed to expand into the flow tube from the fill tank at a regulated pressure.

After depositing the Al_2O_3 ALD and W ALD on the 3M NSTF substrate at 120 °C, the samples were transferred to a plasma-assisted ALD reactor for the Pt ALD at 120 °C.[42] This plasma ALD reactor was equipped with a remote ICP source (Advanced Energy, Ft. Collins, CO). The plasma source was positioned with the opening roughly 3–4 cm above a heated sample stage. The ICP source was a quartz tube (6 cm inner diameter × 25 cm long) surrounded by a copper helical coil. The ICP was generated using a 13.56 MHz RF generator and 50 Ω impedance matching network (Advanced Energy, Ft. Collins, CO). The plasma ALD reactor was pumped by a Pfeiffer TPU 060 turbomolecular pump that was backed by an Alcatel 2010 rotary vane pump. The reactor was separated from the pumping system by a gate valve. This arrangement enabled the Pt precursor to be dosed under static conditions.

B. ALD on TiO_2 nanoparticles and 3M NSTF substrates

TiO_2 nanoparticles (~34 nm APS, Nanophase) with sample sizes of ~0.5 g were coated in the plasma-assisted open-ended rotary reactor. The Al_2O_3 ALD films were grown on the TiO_2 nanoparticles using alternating exposures of trimethylaluminum (TMA) and H_2O at 180 °C. The precursor lines were maintained at ~130 °C to prevent condensation and the TiO_2 nanoparticles were agitated between 160 and 220 RPM to prevent agglomeration. The TMA and H_2O exposures were held under static conditions by closing the gate valve to the pump during precursor dosing. This ensured saturation of the reactions on the high surface area TiO_2 nanoparticles.

The W ALD adhesion layer was grown after the TiO_2 powder was coated with the Al_2O_3 ALD layer. Previous work on W ALD has shown that W ALD nucleates on hydroxylated Al_2O_3 and SiO_2 surfaces after a short delay of 4–10 ALD cycles.[31–35] In contrast, the nucleation behavior of W ALD was examined directly on TiO_2 powder. TEM analysis showed rough and incomplete W ALD films on the TiO_2 nanoparticles without the Al_2O_3 ALD layer. The W ALD was performed using alternating exposures of Si_2H_6 (Voltaix) and WF_6 (Sigma-Aldrich) at 120 °C. After the W ALD and prior to the Pt ALD, the W ALD-coated TiO_2 powder was pretreated using ten 30 s exposures of H_2 plasma at 500 W to remove WF_5* adsorbed species on the W surface.

With a clean W surface, Pt ALD was performed using alternating exposures of $MeCpPtMe_3$ (Strem Chemicals, Inc.) and H_2 (Airgas, UHP) plasma at 150 °C. The $MeCpPtMe_3$ was held in a glass bubbler and maintained at ~50 °C to obtain a 50 mTorr dosing vapor pressure. The plasma exposure was performed for 30 s at 500 W using 65 sccm (~400 mTorr) of H_2 gas. The schematic in Fig. 3 shows the first set of sequential surface reactions during H_2 plasma-assisted growth of Pt ALD on a W ALD adhesion layer.

The 3M NSTF material consists of a layer of oriented organic crystalline whiskers with nanometer dimensions that have been vapor deposited onto a microstructured Kapton sheet with corrugated features.[36–38] Sample sizes of 3 cm × 6 cm were taped to aluminum sheets and placed in the viscous flow reactor. The Al_2O_3 ALD was deposited using 20 cycles of TMA and H_2O at 120 °C. The W ALD was then deposited on the Al_2O_3-coated 3M NSTF using the following sequence: 14 cycles of Si_2H_6 and WF_6, 1 Al_2O_3 ALD cycle, and another 14 cycles of Si_2H_6 and WF_6 at 120 °C. The single Al_2O_3 ALD layer was inserted between the two W ALD layers to break up the W crystallites in the W ALD layer and prevent delamination during fuel cell testing.

The samples coated with Al_2O_3 ALD and W ALD were transferred in air to the plasma-assisted ALD reactor. Prior to Pt ALD, the samples were exposed to the H_2 plasma pretreatment process to reduce the surface oxide to a clean W metal surface. Without the H_2 plasma pretreatment, the Pt ALD films were observed by TEM analysis to be much rougher. The Pt ALD was deposited using alternating exposures of $MeCpPtMe_3$ (Strem Chemicals, Inc.) and H_2 (Airgas, UHP) plasma at 120 °C. The H_2 plasma exposure was performed for 30 s at 100 W using 26 sccm (~80 mTorr) H_2 gas flow.

TEM was performed using a Philips CM100 instrument operated at 80 kV in bright field mode. The TEM characterized the conformality, uniformity, and relative thickness of the Pt ALD films on the TiO_2 nanoparticles. Inductively

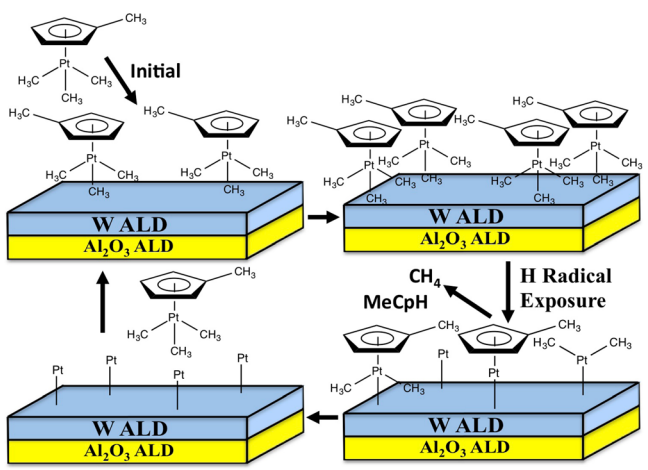

FIG. 3. (Color online) Schematic showing the first set of sequential surface reactions during H_2 plasma-assisted Pt ALD on a W ALD surface.

coupled plasma with optical emission spectroscopy (ICP-OES) and *ex situ* x-ray photoelectron spectroscopy (XPS) were used for elemental analysis. Powder x-ray diffraction (XRD) was performed using a Bruker D2 Phaser instrument operated at 300 W. The XRD was employed to determine the crystal structure of W and Pt ALD. TEM with electron energy loss spectroscopy (EELS) was used to characterize the conformality and elemental composition of the deposited ALD films on the 3M NSTF substrates.

III. REVIEW OF PREVIOUS RESULTS AND INTERPRETATION

The nucleation behavior of Pt ALD films on W ALD adhesion layers was studied earlier by measuring the film thickness and density as a function of the number of ALD cycles using x-ray reflectivity (XRR) analysis.[10] Figure 4 shows Pt ALD film thickness and density measurements up to 1000 ALD cycles.[10] These data show that Pt ALD grown using $MeCpPtMe_3$ with H_2 plasma at 120 °C nucleates rapidly on a W ALD adhesion layer. The inset in Fig. 4 shows that the Pt ALD film reaches a thickness of ~0.75 nm within the first 10 ALD cycles. At this point, the Pt ALD films have a density of only 80%–90% of bulk Pt. This lower density is consistent with the Pt ALD layer forming from the coalescence of Pt nanoclusters. After 100 ALD cycles, the Pt ALD film is ~1.6 nm thick with >95% of the bulk density. This higher density is consistent with closure of the Pt nanoclusters to produce a dense Pt film.

With additional ALD cycles, the Pt film growth rate decreases as the substrate surface shifts from W to Pt.[10] The average growth rate after 1000 ALD cycles is ~0.06 Å per cycle. This growth rate is much lower than the reported value of ~0.45 Å per cycle for both thermal and plasma-assisted Pt ALD using $MeCpPtMe_3$ and O_2.[26,46–50] This slower growth rate is attributed to the differences in growth mechanism using reductive chemistry with the H_2 plasma. In addition, the separation distance between the ICP source and the sample stage may limit the H radical flux.

The rapid nucleation of Pt ALD on W ALD adhesion layers observed during the first 50 ALD cycles was also confirmed by previous XPS analysis.[10] Figure 5 shows the relative XPS atomic fraction from Pt_{4d} and W_{4f} signals versus the density-adjusted Pt ALD film thickness as measured by XRR.[10] Figure 5 shows that a decrease in the relative W_{4f} XPS signal is concurrent with an increase in the Pt_{4d} XPS signal with Pt ALD film growth.[10] The low relative XPS atomic fraction of Pt in the first 0.5 nm is consistent with the initial nucleation of Pt nanoclusters. When the Pt ALD film thickness reaches ~1.5 nm, a transition occurs to layer-by-layer growth. At this point, the Pt ALD films reach densities that are >95% of bulk Pt. The predicted layer-by-layer growth of Pt closely matches the experimental measurements after a Pt film thickness of ~1.5 nm.

The rapid nucleation of Pt ALD on W ALD adhesion layers was confirmed by previous *in situ* spectroscopic ellipsometry (SE) measurements.[42] Figure 6 shows the Pt ALD thickness versus the number of ALD cycles using $MeCpPtMe_3$ and H_2 plasma at 120 °C.[42] The plasma exposure was performed using 11 mTorr of H_2 gas at 100 W for 10 s. These data show that the Pt ALD film growth nucleates immediately and a linear fit to the data yields a growth rate of ~0.23 Å/cycle.[42] This growth rate may be higher than the earlier Pt ALD growth rates determined by the XRR and XPS studies[10] because of the shorter distance between the H_2 plasma source and the substrate.

Further analysis of these samples using *ex situ* XRR and XPS confirmed the rapid nucleation and growth rate of the Pt ALD on W ALD adhesion layers.[42] Figure 7 shows that the Pt ALD film thicknesses measured by *in situ* SE closely match the Pt ALD film thicknesses measured by *ex situ* XRR

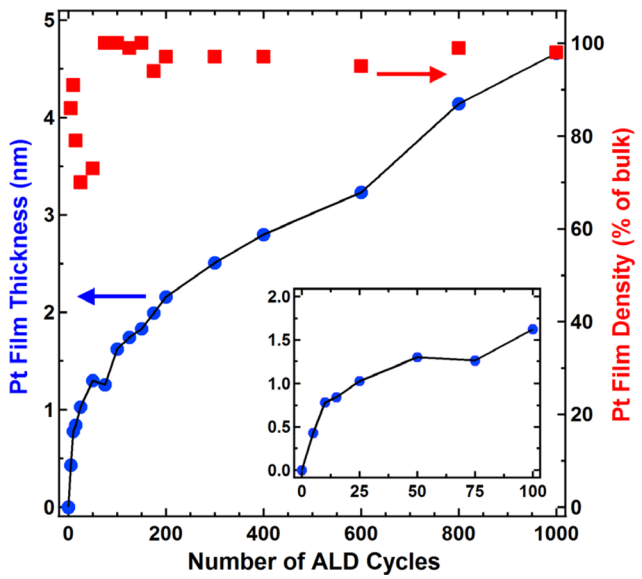

FIG. 4. (Color online) Pt ALD film thickness and density from XRR measurements vs the number of Pt ALD cycles on W ALD adhesion layers. Reprinted with permission from Baker *et al.*, Appl. Phys. Lett. **101**, 111601 (2012). Copyright 2012, American Institute of Physics.

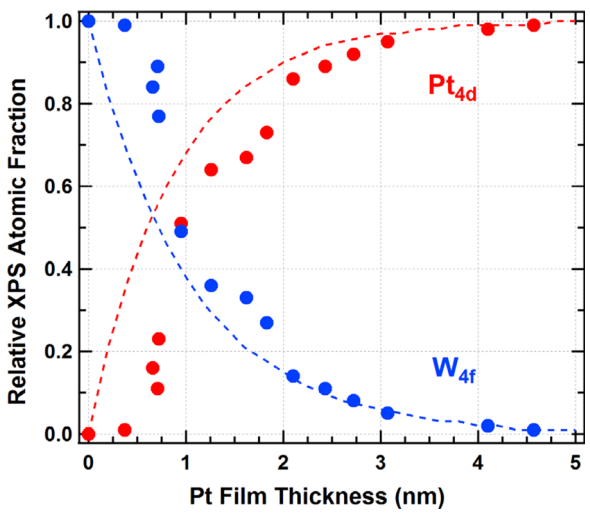

FIG. 5. (Color online) Relative XPS atomic fractions from Pt_{4d} and W_{4f} XPS signals vs Pt ALD film thickness on W ALD adhesion layers. The dashed lines represent predictions from a layer-by-layer growth model. Reprinted with permission from Baker *et al.*, Appl. Phys. Lett. **101**, 111601 (2012). Copyright 2012, American Institute of Physics.

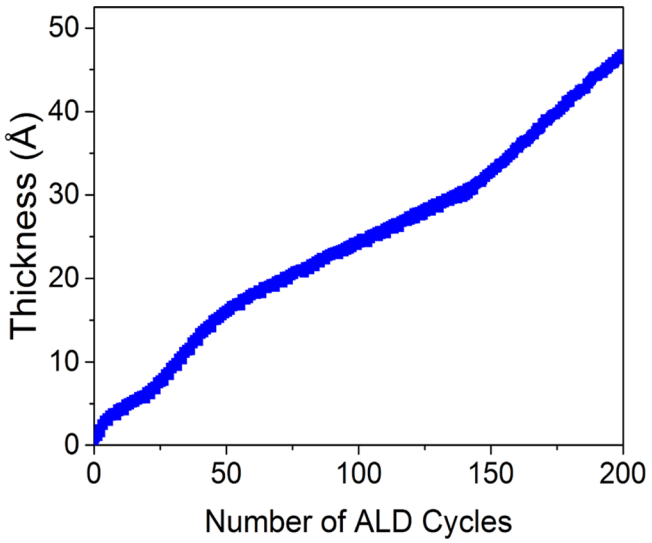

FIG. 6. (Color online) Pt film thickness measured by *in situ* spectroscopic ellipsometry (SE) vs the number of Pt ALD cycles on W ALD adhesion layers. The estimated Pt ALD growth rate is ~0.23 Å/cycle. Adapted with permission from Cavanagh *et al.*, ECS Trans. **58**, 19 (2013). Copyright 2013, The Electrochemical Society.

and XPS.[42] The *ex situ* XPS and XRR data confirm a growth rate of ~0.2 Å per cycle. Figure 7 also shows that the Pt ALD films reach a density of 100% of bulk Pt after ~50 ALD cycles at a film thickness of ~1.5 nm. These results are in excellent agreement with the results in Fig. 4.

The demonstration of ultrathin and continuous Pt ALD films at a thickness of ~1.5 nm is significant because existing methods of Pt ALD only yield continuous films at thicknesses of ~10–20 nm.[26,46–50] Such Pt ALD films are too thick to be used in applications such as fuel cell catalysts where the Pt must be used as efficiently as possible to be cost effective and useful. At these larger Pt film thicknesses, the benefit of the 5–10 fold higher area-specific activity of large radius of curvature Pt surfaces is lost. Too much underlying Pt is required to support the larger radius of curvature Pt surface.

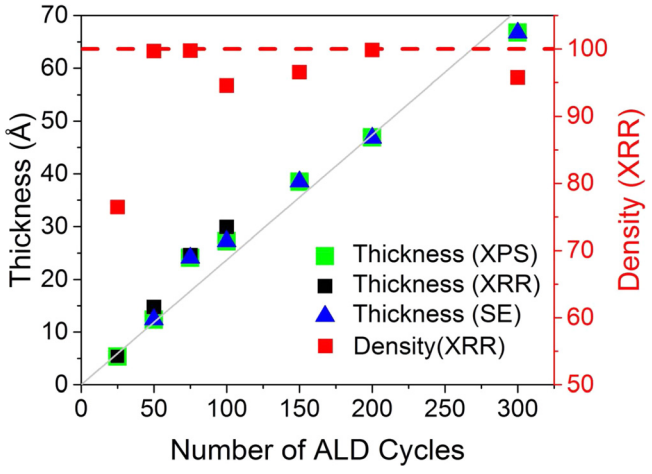

FIG. 7. (Color online) Pt ALD film thickness and density measured by *in situ* SE and *ex situ* XPS and XRR vs the number of Pt ALD cycles. Adapted with permission from Cavanagh *et al.*, ECS Trans. **58**, 19 (2013). Copyright 2013, The Electrochemical Society.

The W ALD adhesion layer facilitates the growth of continuous Pt ALD films. These Pt ALD films have the density of bulk Pt at a Pt ALD thickness of ~1.5 nm. The high surface energy of the W ALD layer allows the Pt ALD film to "wet" the W ALD layer. This wetting behavior can be understood using Young's equation. If the initial Pt nanoclusters that form during nucleation are treated as liquid droplets on a solid surface, Young's equation can provide a qualitative explanation for the relationship between surface energies and the wetting behavior.[51]

Equation (1) presents Young's equation where S designates the substrate, L designates a liquid droplet on the substrate, SL is the substrate–liquid interface, and Θ is the contact angle

$$\gamma_S = +\gamma_L(\cos\,\theta) + \gamma_{SL}. \quad (1)$$

In this application of Young's equation, γ_S is the surface energy of the substrate. γ_L is the surface energy of the Pt nanocluster "droplet." γ_{SL} is the interfacial energy between the substrate and Pt nanocluster "droplet." θ is the contact angle of the Pt nanocluster "droplet" on the substrate.

For ideal wetting behavior, $\Theta \approx 0$ and $\cos\Theta \approx 1$. Under these circumstances, Young's equation becomes $\gamma_S = +\gamma_L + \gamma_{SL}$. Assuming a finite interfacial energy, wetting demands that $\gamma_S > \gamma_L$. Therefore, the underlying substrate has a higher surface energy than the liquid "droplet" on the substrate. For this application of Pt ALD on W ALD adhesion layers, the surface energy for the W ALD film must be larger than the surface energy for the Pt nanocluster "droplet."

In another interpretation of the results, the Pt ALD film will coat the W ALD adhesion layer because the Pt ALD film has a lower surface energy than the W ALD film. Thermodynamically, the lower surface energy of the Pt ALD film is favored on the W ALD adhesion layer because the Pt ALD coating reduces the surface energy. This interpretation assumes that the interfacial energy between the Pt ALD film and the W ALD adhesion layer is not a significant factor.

IV. RESULTS ON HIGH SURFACE AREA SUBSTRATES AND DISCUSSION

A continuous and ultrathin Pt layer on a high surface area support is an ideal catalytic surface for the ORR in PEM fuel cells. Having a continuous Pt film increases resistance to dissolution and Ostwald ripening mechanisms.[1,3,46–50] A Pt film with a high radius of curvature also yields a higher area-specific activity compared with Pt nanoparticles.[1,3] TiO_2 nanoparticles and 3M NSTF were chosen as two diverse substrate materials to demonstrate the method for depositing ultrathin and continuous Pt ALD films. These two support materials are ideal because they are inexpensive, offer high electrochemical corrosion resistance, and provide a large surface area.[1,36–41]

A. TiO_2 nanoparticle substrates

A conformal and continuous ultrathin Pt ALD film on high surface area TiO_2 nanoparticles requires a uniform and

continuous W ALD adhesion layer. Although W has a very high surface energy, W ALD is observed to grow as an ultrathin and continuous film on Al_2O_3 ALD surfaces.[31] This growth may be attributed to the favorable thermodynamics of AlF_3 formation upon exposure of the Al_2O_3 surface to the WF_6 precursor during W ALD.[52] This explanation is also consistent with our observation of a significant drop in transient pressure during the first static dose of WF_6. This drop in pressure may result from the uptake of WF_6 into the Al_2O_3 film to form AlF_3 at the film surface. Based on this mechanism, we first deposit a thin and conformal Al_2O_3 ALD film on the TiO_2 nanoparticles to provide a seed layer for optimal nucleation of the W ALD adhesion layer.

Figure 8 displays a TEM image that shows a thin and conformal Al_2O_3 ALD film deposited on the TiO_2 nanoparticles using 23 cycles of TMA and H_2O at 180 °C. The Al_2O_3 ALD film thickness is ~27 Å. The growth rate of ~1.2 Å per cycle obtained from the film thickness is consistent with reported values for Al_2O_3 ALD.[53,54] The presence of Al_2O_3 on the TiO_2 nanoparticles was confirmed using XPS and ICP-OES analysis. The Al_2O_3 ALD seed layer was then followed by 30 cycles of W ALD.

Figure 9 displays a TEM image after 30 cycles of W ALD deposited at 120 °C on TiO_2 nanoparticles that were previously coated with 23 cycles of Al_2O_3 ALD. In comparison to the TEM image in Fig. 8, the W ALD film in Fig. 9 yields a much darker image. The dark image is consistent with more electron scattering from a more electron dense W film. The presence of W was also confirmed by both *ex situ* XPS and ICP-OES analyses. The W ALD film is uniform and conformal to the underlying Al_2O_3 ALD-coated TiO_2 nanoparticles. The appearance of a dark ring around the particles in Fig. 8 is attributed to an edge effect of the electron

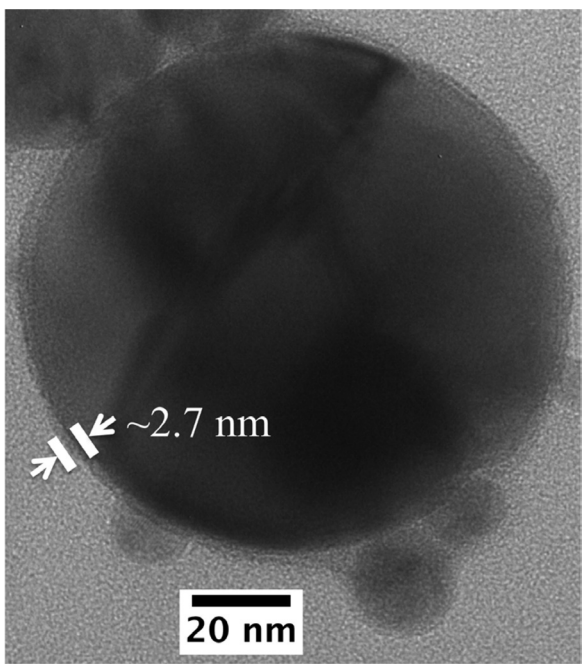

FIG. 8. TEM image of 23 Al_2O_3 ALD cycles on TiO_2 nanoparticles at 180 °C. The Al_2O_3 ALD film is ~2.7 nm thick corresponding to a Al_2O_3 ALD growth rate of ~1.2 Å per cycle.

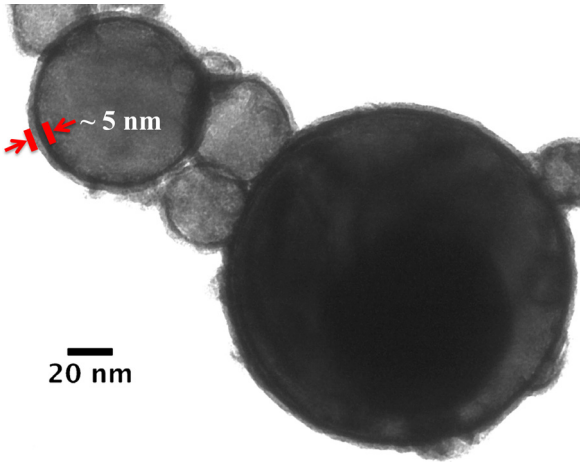

FIG. 9. (Color online) TEM image of TiO_2 nanoparticles coated with 23 Al_2O_3 ALD cycles at 180 °C and 30 W ALD cycles at 120 °C. The W ALD film is ~5 nm thick corresponding to a W ALD growth rate of ~1.7 Å per cycle.

dense W ALD coating on the nearly spherical TiO_2 particles. The electron beam interacts with a larger amount of the W ALD layer as the electron beam passes through the W ALD coating on the curved edge of the TiO_2 particle. This increased electron scattering results in the appearance of a dark ring.

The estimated W ALD film thickness from the TEM image in Fig. 9 is ~5 nm. This W ALD thickness corresponds to a W ALD growth rate of ~1.7 Å per cycle. This growth rate is somewhat lower than the typical linear growth rate of ~3.5 Å per cycle for W ALD.[31–35] However, the W ALD growth rate is observed to change depending on the reaction temperature and Si_2H_6 exposure.[31] Powder XRD analysis of the W and Al_2O_3 ALD-coated TiO_2 nanoparticles revealed no crystallinity from the Al_2O_3 ALD layer. The XRD analysis did observe the presence of the crystalline α-W phase with a single strong (110) diffraction peak at $2\theta = 40°$.

The H_2 plasma exposure was used to establish a pristine W surface prior to the Pt ALD step. The H_2 plasma exposure helps remove the WF_5* surface species that remain on the W ALD surface after the last WF_6 exposure of the 30 W ALD cycles. The H_2 plasma exposure also helps to reduce any oxide that may have formed on the W ALD surface. The H_2 plasma treatment was performed using ten 30 s exposures of H_2 plasma at 500 W. The H_2 plasma pretreatment was then followed by 215 cycles of Pt ALD.

Figure 10 shows a TEM image after 215 cycles of Pt ALD at 150 °C on the W and Al_2O_3 ALD-coated TiO_2 nanoparticles. The Pt ALD film is continuous and conformal to the TiO_2 particles. From the TEM image, the Pt ALD films are estimated to be ~4 nm thick after subtracting the underlying ~5 nm W ALD film. This Pt ALD film thickness corresponds to a growth rate of ~0.19 Å/cycle. This growth rate closely matches the growth rates of ~0.23 Å/cycle obtained from *in situ* SE analysis and ~0.2 Å/cycle from *ex situ* XPS and XRR measurements.[42] The presence of Pt metal was also confirmed using *ex situ* XPS and ICP-OES analyses.

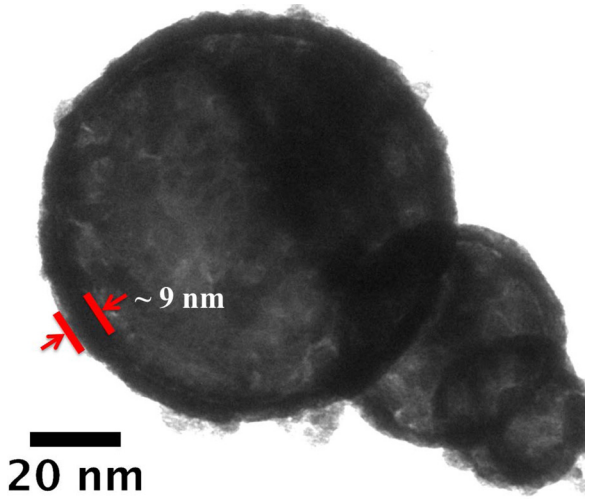

FIG. 10. (Color online) TEM image of 215 Pt ALD cycles on TiO_2 nanoparticles at 150 °C coated previously with 23 Al_2O_3 ALD cycles at 180 °C and 30 W ALD cycles at 120 °C. The Pt ALD film is ~4 nm thick after subtracting the underlying ~5 nm W ALD film. This Pt ALD film thickness corresponds to a Pt ALD growth rate of 0.19 Å/cycle.

Compared with the W and Al_2O_3 ALD-coated TiO_2 nanoparticles, powder XRD analysis of the Pt ALD on the W and Al_2O_3 ALD-coated TiO_2 nanoparticles revealed an increased diffraction peak signal at $2\theta = 40°$ corresponding with the (110) diffraction peak from α-W. The absence of the other notable Pt diffraction signals, such as the (200), (220), and (311) diffraction peaks, suggests that the Pt ALD has grown epitaxially on the W(110) surface. The other diffraction peaks are not observed because the ultrathin Pt ALD layer epitaxially grown on W(110) is only thick enough to yield the (110) diffraction feature. The epitaxial growth of Pt on W(110) and W(111) surfaces has been observed in earlier single-crystal studies.[55,56]

The W ALD adhesion layer is critical to deposit continuous and ultrathin Pt ALD films. To illustrate this point, TEM images compared the difference in Pt ALD film morphology between TiO_2 samples with and without the W ALD adhesion layer. When the W ALD adhesion layer was present after 30 W ALD cycles, the Pt ALD nucleates rapidly leading to a continuous Pt ALD film that is conformal to the TiO_2 nanoparticle substrate as shown in Fig. 11(a). When the W ALD adhesion layer is not present prior to the plasma-assisted Pt ALD, the formation of discrete Pt nanoparticles is observed as shown in Fig. 11(b). The TiO_2 nanoparticles in Fig. 11(b) were coated only with 23 cycles of Al_2O_3 ALD prior to the Pt ALD. Pt nanoparticles are usually observed during Pt ALD on low surface energy metal oxide substrates.[14–27] These TEM images clearly illustrate the difference between Pt ALD growth on high and low surface energy surfaces.

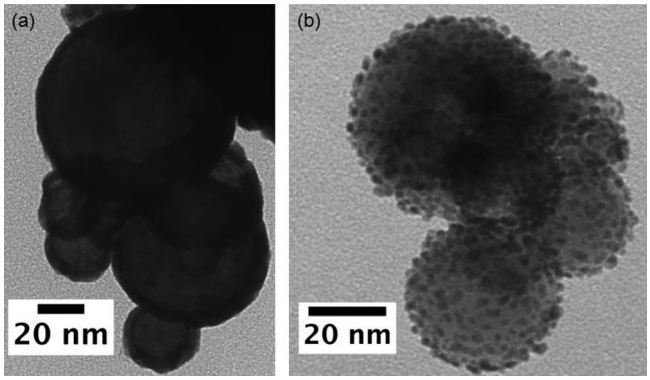

FIG. 11. TEM images after 215 Pt ALD cycles at 150 °C on: (a) TiO_2 nanoparticles that were coated with 23 Al_2O_3 ALD cycles at 180 °C and 30 W ALD cycles at 120 °C. (b) TiO_2 nanoparticles that were coated with only 23 Al_2O_3 ALD cycles at 180 °C. The W ALD adhesion layer yields continuous and conformal Pt ALD films.

B. 3M NSTF substrates

Continuous and ultrathin Pt ALD films were also grown on 3M NSTF substrates at 120 °C using a high surface energy W ALD adhesion layer. The 3M NSTF substrates are organic molecular solids in the form of oriented crystalline "whiskers" on a Kapton microstructured backing.[1,36–38] The

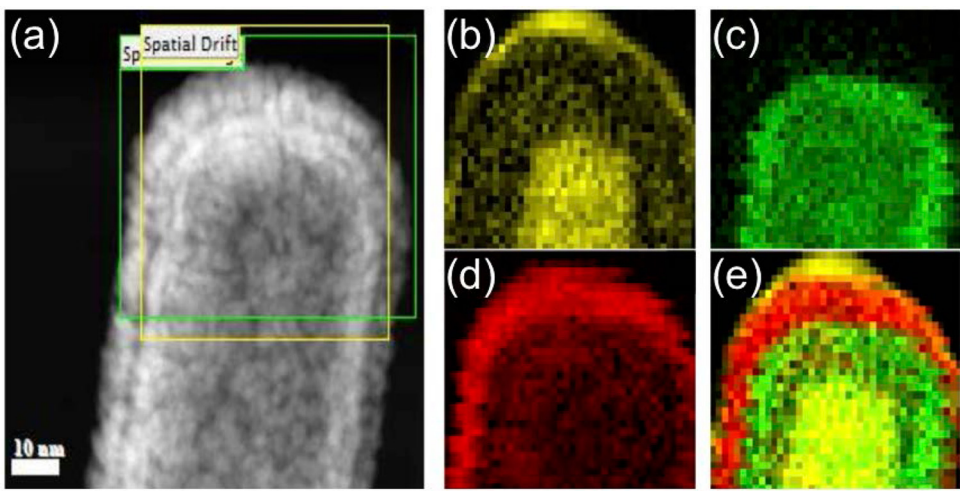

FIG. 12. (Color online) (a) TEM image of a single NSTF whisker coated with 150 Pt ALD cycles after 20 Al_2O_3 ALD cycles and 28 W ALD cycles. All depositions were performed at 120 °C. TEM-EELS images show individual elemental mapping of: (b) carbon, (c) W, and (d) Pt. (e) Overlay of TEM-EELS images for the three elements.

whiskers have nanometer dimensions and are both thermally and electrochemically stable. The 3M NSTF substrates are potential candidates for electrodes for PEM fuel cells.

The 3M NSTF substrates were initially coated with 20 cycles of Al_2O_3 ALD to establish a seed layer for the W ALD layer at 120 °C. Subsequently, the W ALD adhesion layer was deposited using two sequences of {14 W ALD cycles, 1 Al_2O_3 ALD cycle} at 120 °C. The ultrathin Pt ALD film was then deposited using 150 cycles of Pt ALD at 120 °C.

Figure 12 shows the TEM and TEM–EELS images of the coated 3M NSTF substrates. The W and Pt ALD films are uniform and highly conformal to the 3M NSTF whiskers. Figure 12(a) shows the TEM image of a single NSTF whisker. Figures 12(b)–12(d) show the EELS images for carbon, tungsten and platinum, respectively. Figure 12(e) displays an overlay of all the elements.

Figure 12 indicates that the Pt and W ALD coatings are continuous and conformal on the NSTF substrate. The Pt and W ALD film thicknesses from Figs. 12(c) and 12(d) are estimated to be ~4 nm. The small amount of adventitious carbon observed on top of the NSTF substrate on the ultrathin Pt ALD film is believed to result from air exposure prior to the *ex situ* TEM-EELS analysis.[57–59]

V. CONCLUSIONS

Continuous and ultrathin Pt ALD films can be deposited on flat and high surface area substrates using W ALD as a high surface energy adhesion layer. A review of previous XRR and XPS studies showed that the Pt ALD grows with a layer-by-layer growth mode. In addition, the Pt film density is >95% of the density of bulk Pt at a Pt ALD film thickness of ~1.5 nm. Further evidence for the rapid nucleation of Pt ALD on W ALD adhesion layers was provided by SE analysis in conjunction with XRR and XPS analysis. The SE results showed immediate nucleation of Pt ALD growth on the W ALD adhesion layer with a Pt ALD growth rate of ~0.23 Å per cycle. This growth rate was consistent with the XPS and XRR measurements.

Continuous and ultrathin Pt ALD films were also deposited on high surface area TiO_2 nanoparticle and 3M NSTF substrates. TiO_2 nanoparticles were conformally coated with a sequence of ~2.7 nm Al_2O_3 ALD, ~5 nm W ALD, and ~4 nm Pt ALD, as estimated from TEM images. *Ex situ* XPS and ICP-OES confirmed the presence of Al_2O_3, W, and Pt. The Pt ALD film growth rate on the coated TiO_2 nanoparticles was estimated to be ~0.19 Å per cycle. TEM-EELS analysis of the ALD-coated 3M NSTF substrate indicated that the ~4 nm thick W and Pt ALD films were very uniform and conformal to the NSTF whisker. The deposition of these continuous and ultrathin Pt ALD films on high surface area substrates may help to reduce Pt catalyst loading in PEM fuel cells.

ACKNOWLEDGMENTS

This research was funded by General Motors Research and Development and the Defense Advanced Research Project Agency (DARPA). The authors would like to thank Advanced Energy, Inc., for providing the plasma sources used in this work. The authors also thank Mark K. Debe, Edward M. Fischer, and Andrew Steinbach of 3M for providing the NSTF samples.

[1]R. Borup *et al.*, Chem. Rev. **107**, 3904 (2007).
[2]S. S. Kocha, "Principles of MEA preparation," in *Handbook of Fuel Cells—Fundamentals, Technology and Applications*, edited by W. Vielstich, A. Lamm, and H. Gasteiger (Wiley, Chichester, 2003), Vol. 3, Chap. 43, p. 538.
[3]H. A. Gasteiger, S. S. Kocha, B. Sompalli, and F. T. Wagner, Appl. Catal., B **56**, 9 (2005).
[4]M. K. Debe, Nature **486**, 43 (2012).
[5]F. T. Wagner, B. Lakshmanan, and M. F. Mathias, J. Phys. Chem. Lett. **1**, 2204 (2010).
[6]Y. Shao-Horn, W. C. Sheng, S. Chen, P. J. Ferreira, E. F. Holby, and D. Morgan, Top. Catal. **46**, 285 (2007).
[7]Z. Wang, P. Zuo, Y. Chu, Y. Shao, and G. Yin, Int. J. Hydrogen Energy **34**, 4387 (2009).
[8]X. Yu and S. Ye, J. Power Sources **172**, 145 (2007).
[9]S. Chen, H. A. Gasteiger, K. Hayakawa, T. Y. Tada, and Y. Shao-Horn, J. Electrochem. Soc. **157**, A82 (2010).
[10]L. Baker, A. S. Cavanagh, J. Yin, S. M. George, A. Kongkanand, and F. T. Wagner, Appl. Phys. Lett. **101**, 111601 (2012).
[11]R. L. Puurunen, J. Appl. Phys. **97**, 121301 (2005).
[12]S. M. George, Chem. Rev. **110**, 111 (2010).
[13]H. B. Profijt, S. E. Potts, M. C. M. van de Sanden, and W. M. M. Kessels, J. Vac. Sci. Technol., A **29**, 050801 (2011).
[14]L. Baker, A. S. Cavanagh, D. Seghete, S. M. George, A. J. M. Mackus, W. M. M. Kessels, Z. Y. Liu, and F. T. Wagner. J. Appl. Phys. **109**, 084333 (2011).
[15]S. T. Christensen, J. W. Elam, B. Lee, Z. Feng, M. J. Bedzyk, and M. C. Hersam, Chem. Mater. **21**, 516 (2009).
[16]S. T. Christensen *et al.*, Small **5**, 750 (2009).
[17]A. Goulas and J. R. van Ommen, J. Mater. Chem. A **1**, 4647 (2013).
[18]W. Setthapun *et al.*, J. Phys. Chem. C **114**, 9758 (2010).
[19]Y. Zhou, D. M. King, X. Liang, J. Li, and A. W. Weimer, Appl. Catal. B **101**, 54 (2010).
[20]Y. Lei *et al.*, Chem. Mater. **24**, 3525 (2012).
[21]J. A. Enterkin, K. R. Poeppelmeier, and L. D. Marks, Nano Lett. **11**, 993 (2011).
[22]Y. H. Lin, Y. C. Hsueh, C. C. Wang, J. M. Wu, T. P. Perng, and H. C. Shih, Electrochem. Solid-State Lett. **13**, K93 (2010).
[23]S. Novak, B. Lee, X. Y. Yang, and V. Misra, J. Electrochem. Soc. **157**, H589 (2010).
[24]M. J. Weber, A. J. M. Mackus, M. A. Verheijen, C. van der Marel, and W. M. M. Kessels, Chem. Mater. **24**, 2973 (2012).
[25]J. H. Li, X. H. Liang, D. M. King, Y. B. Jiang, and A. W. Weimer, Appl. Catal., B **97**, 220 (2010).
[26]T. Aaltonen, M. Ritala, T. Sajavaara, J. Keinonen, and M. Leskela, Chem. Mater. **15**, 1924 (2003).
[27]V. R. Anderson, N. Leick, J. W. Clancey, K. E. Hurst, K. M. Jones, A. C. Dillon, and S. M. George, J. Phys. Chem. C **118**, 8960 (2014).
[28]C. T. Campbell, Surf. Sci. Rep. **27**, 1 (1997).
[29]S. H. Overbury, P. A. Bertrand, and G. A. Somorjai, Chem. Rev. **75**, 547 (1975).
[30]L. Vitos, A. V. Ruban, H. L. Skriver, and J. Kollar, Surf. Sci. **411**, 186 (1998).
[31]R. W. Wind, F. H. Fabreguette, Z. A. Sechrist, and S. M. George, J. Appl. Phys. **105**, 074309 (2009).
[32]J. W. Elam, C. E. Nelson, R. K. Grubbs, and S. M. George, Thin Solid Films **386**, 41 (2001).
[33]J. W. Elam, C. E. Nelson, R. K. Grubbs, and S. M. George, Surf. Sci. **479**, 121 (2001).
[34]J. W. Klaus, S. J. Ferro, and S. M. George, Thin Solid Films **360**, 145 (2000).
[35]R. K. Grubbs, C. E. Nelson, N. J. Steinmetz, and S. M. George, Thin Solid Films **467**, 16 (2004).
[36]M. K. Debe, ECS Trans. **45**, 47 (2012).
[37]M. K. Debe, R. T. Atanasoski, and A. J. Steinbach, ECS Trans. **41**, 937 (2011).

[38]M. K. Debe, A. K. Schmoeckel, G. D. Venstrom, and R. Atanasoski, J. Power Sources **161**, 1002 (2006).
[39]Y. Shao, J. Liu, Y. Wang, and Y. Lin, J. Mater. Chem. **19**, 46 (2009).
[40]T. Ioroi, Z. Siroma, N. Fujiwara, S. Yamazaki, and K. Yasuda, Electrochem. Commun. **7**, 183 (2005).
[41]J. E. Graves, D. Pletcher, R. L. Clarke, and F. C. Walsh, J. Appl. Electrochem. **21**, 848 (1991).
[42]A. S. Cavanagh, L. Baker, J. W. Clancey, J. Yin, A. Kongkanand, F. T. Wagner, and S. M. George, ECS Trans. **58**, 19 (2013).
[43]J. A. McCormick, B. L. Cloutier, A. W. Weimer, and S. M. George, J. Vac. Sci. Technol., A **25**, 67 (2007).
[44]J. A. McCormick, K. P. Rice, D. F. Paul, A. W. Weimer, and S. M. George, Chem. Vap. Deposition **13**, 491 (2007).
[45]D. Longrie, D. Deduytsche, J. Haemers, K. Driesen, and C. Detavernier, Surf. Coat. Technol. **213**, 183 (2012).
[46]X. Jiang and S. F. Bent, J. Electrochem. Soc. **154**, D648 (2007).
[47]X. Jiang, H. Huang, F. B. Prinz, and S. F. Bent, Chem. Mater. **20**, 3897 (2008).
[48]H. C. M. Knoops, A. J. M. Mackus, M. E. Donders, M. C. M. van de Sanden, P. H. L. Notten, and W. M. M. Kessels, Electrochem. Solid-State Lett. **12**, G34 (2009).
[49]J. Hamalainen, F. Munnik, M. Ritala, and M. Leskela, Chem. Mater. **20**, 6840 (2008).
[50]J. Hamalainen, M. Ritala, and M. Leskala, Chem. Mater. **26**, 786 (2014).
[51]A. W. Adamson and A. P. Gast *Physical Chemistry of Surfaces*, 6th ed. (Wiley, New York, 1997).
[52]F. H. Fabreuguette, Z. A. Sechrist, J. W. Elam, and S. M. George, Thin Solid Films **488**, 103 (2005).
[53]S. M. George, A. W. Ott, and J. W. Klaus, J. Phys. Chem. **100**, 13121 (1996).
[54]M. D. Groner, F. H. Fabreguette, J. W. Elam, and S. M. George, Chem. Mater. **16**, 639 (2004).
[55]J. J. Kolodziej, T. E. Madey, J. W. Keister, and J. E. Rowe, Phys. Rev. B **65**, 075413 (2002).
[56]S. M. Shivaprasad, R. A. Demmin, and T. E. Madey, Thin Solid Films **163**, 393 (1988).
[57]T. L. Barr and S. Seal, J. Vac. Sci. Technol., A **13**, 1239 (1995).
[58]L. R. Merte, M. Ahmadi, F. Behafarid, L. K. Ono, E. Lira, J. Matos, L. Li, J. C. Yang, and B. R. Cuenya, ACS Catal. **3**, 1460 (2013).
[59]S. Proch, M. Wirth, H. S. White, and S. L. Anderson, J. Am. Chem. Soc. **135**, 3073 (2013).